

Evaluation of Equivalent Dynamic Active Distribution Network Models with Individual and Aggregated Consideration of Grid Forming Converters

Jakob Ungerland* and Hendrik Lens

Detailed active distribution network modeling in the context of stability studies of future power systems can be avoided by applying complexity-reduced equivalent dynamic models. Previous work developed an approach to derive such equivalent dynamic network models of systems dominated by grid following and grid forming converters. Nevertheless, this approach lacks an investigation of the aggregation of multiple grid forming converters to one equivalent component. Also, the approach needs to be evaluated for a closed ring topology to substantiate its validity independent of the detailed network topology. This work applies and validates the developed approach on active distribution networks in the context of three scenarios. The detailed and equivalent network models are simulated for three events and the results are used to compare the models with respect to accuracy and complexity. The derived equivalent dynamic network models with an individual representation of grid forming converters reproduce the dynamic behavior of the corresponding detailed networks very well. The aggregation of grid forming converters results in an adequate reproduction of the detailed network's dynamic behavior under the constraint of aggregating only neighboring grid forming converters of one branch. This allows for the consideration of the detailed network's topology in the corresponding equivalent dynamic model.

development of active distribution networks (ADN) and diminishes the importance of conventional generation, mostly located in the transmission system, for power system stability. Hence, stability analysis of CBG-dominated systems needs to consider the dynamic behavior of such ADN. Nevertheless, an implementation of detailed ADN models in transmission system models used for stability analysis results in a complex overall model that requires high computational resources.

An equivalent dynamic ADN model (EDAM) substituting a detailed ADN model can reproduce the dynamic behavior of the detailed model at the connecting bus of the ADN to the transmission system. This connecting bus is called boundary bus. It is crucial that EDAM reproduce the dynamic behavior of the corresponding detailed ADN with sufficient accuracy while significantly reducing its complexity. The creation of EDAM for future CBG-dominated ADN has been addressed by gray- or black-box approaches that are based on data obtained

from a large number of simulations, such as in refs. [1–3], and by clustering-based approaches, as presented in refs. [4,5]. See Section 1.2.1 for further details on these different types of EDAM.

For stability analysis of future power systems containing mostly CBG in ADN, grid forming converters (GFMC) play a significant role.^[6] Opposed to conventional grid following converters (GFLC), GFMC emulate key properties of synchronous machines in the sense that they act as an AC voltage source equipped with inertia and, thus, stabilize the system. Hence, EDAM that consider the dynamic behavior of GFMC properly become increasingly important for stability analysis.

As simulation-based approaches are computationally heavy due to the high number of simulations that is necessary, and clustering-based approaches generally do not consider GFMC, there is a need for a clustering-based approach that is capable of considering GFMC in EDAM to render comprehensive stability analysis possible. This need has been addressed in previous work.^[7] There, the so-called Sensitivity-Technology-Control-Clustered Approach (STCA) has been introduced, which yields EDAM that can reproduce the dynamic behavior of GFMC adequately. In this article, an EDAM aggregated by STCA is referred to as a STCA-EDAM.

While ref. [7] is, to the knowledge of the authors, the first clustering-based algorithm that incorporates GFMC, the analysis


1. Introduction

1.1. Motivation

Increasing penetration of converter-based generation (CBG), mostly located in distribution systems, expedites the

J. Ungerland
Smart Grids
Fraunhofer Institute for Solar Energy Systems ISE
79110 Freiburg, Germany
E-mail: jakob.ungerland@ise.fraunhofer.de

H. Lens
Institute of Combustion and Power Plant Technology
University of Stuttgart
70569 Stuttgart, Germany

 The ORCID identification number(s) for the author(s) of this article can be found under <https://doi.org/10.1002/ente.202300336>.

© 2023 The Authors. Energy Technology published by Wiley-VCH GmbH. This is an open access article under the terms of the Creative Commons Attribution License, which permits use, distribution and reproduction in any medium, provided the original work is properly cited.

DOI: 10.1002/ente.202300336

there is limited to ADN that comprise the same number of GFMC elements as the detailed ADN model, i.e., six GFMC in the ADN model considered. With an increasing number of GFMC in the detailed ADN model, aggregating multiple GFMC to one equivalent GFMC in the STCA-EDAM becomes relevant because the complexity of the resulting EDAM can be reduced. Also, the application of STCA in ref. [7] is limited to an open ring network topology. However, around 15% of the medium voltage networks in Germany are operated as closed ring topologies.^[8] Hence, in addition to the aggregation of multiple GFMC, this work also evaluates the STCA further with respect to its application on different ADN topologies.

1.2. Equivalent Dynamic ADN Models

1.2.1. Classification

As introduced in refs. [7,9] and based on the classification by previous studies,^[10–13] methods to create EDAM can be categorized in methods for networks with conventional generation only, i.e., coherency and modal-based approaches,^[14,15] and for networks with both conventional generation and CBG. The latter is relevant for stability studies of future power systems dominated by CBG. These methods utilize parameter identification methods to either parameterize a gray-box or black-box model. The former can be further categorized into clustering-based and generic model-based approaches, e.g., as introduced in refs. [1,3,16–22]. The latter utilizes deep learning to train an artificial neural network, e.g., as published in refs. [2,23]. Both generic model-based gray-box and black-box approaches require comprehensive input data for the parameterization algorithms. Also, parameterizing such an EDAM requires high computational resources.

These drawbacks can be avoided by utilizing clustering-based gray-box approaches.^[4,5,24] Dependent on detailed information on the ADN, EDAM can be obtained without high computational effort. Nevertheless, insight into the ADN model to be aggregated is required, which makes it difficult to use these approaches to model real ADN. However, for stability analysis of future power systems, representative expected ADN structures are sufficient. For such a use case, it is therefore reasonable to assume that a detailed dynamic model of the ADN that is to be aggregated is available.

1.2.2. Technology-Control-Clustered Approach

Previous work identifies the Technology-Control-Clustered Approach (TCA) developed by Bömer^[5] as a promising clustering-based gray-box approach to derive EDAM of CBG-dominated systems.^[25] This work refers to an EDAM aggregated by TCA as a TCA-EDAM. As soon as GFMC are implemented in the ADN, the corresponding TCA-EDAM is not capable of reproducing the dynamic behavior of the corresponding detailed network adequately.^[7] For benchmarking purposes, the TCA is applied on the considered ADN in this work.

A TCA-EDAM is derived by clustering the detailed network's components according to technology, control strategy, and voltage level.^[5] Based on the respective cluster, equivalent components are created and connected to one equivalent busbar per voltage level

cluster. The links between voltage levels comprise equivalent transformers and impedances. The latter are parameterized such that the steady-state power flow at the boundary bus of the EDAM is close to the power flow at the boundary bus of the detailed ADN.

1.2.3. Sensitivity-Technology-Control-Clustered Approach

All equivalent components of one voltage level are connected to the same equivalent busbar in a TCA-EDAM. Such an aggregation neglects the grid's strength at each node of the detailed network. The dynamic behavior of GFMC, however, depends on the grid's strength and cannot be captured adequately in a TCA-EDAM.

This drawback is addressed by the STCA as introduced in ref. [7]. This approach clusters the detailed network's components similar to the TCA. Additionally, each equivalent GFMC is connected to the lower voltage side of the equivalent transformer with an individual equivalent impedance according to the detailed network's topology. The individual representation of each detailed network's GFMC in the EDAM is needed to consider the network topology in the EDAM. Each equivalent impedance is parameterized such that the voltage sensitivities $\frac{\partial V_i}{\partial P_i}$, $\frac{\partial V_i}{\partial Q_i}$, $\frac{\partial \theta_i}{\partial P_i}$, and $\frac{\partial \theta_i}{\partial Q_i}$ of the equivalent GFMC i are similar to those at the point of common coupling (PCC) of the corresponding GFMC in the detailed network. Such a parameterization ensures a consideration of the grid's strength at the PCC of the equivalent GFMC. The active and reactive nominal power values of the equivalent GFMC are the summation of the active and reactive nominal power values of the GFMC per cluster in the detailed network. The equivalent GFMC control parameters are the same as the GFMC control parameters of the respective cluster in the detailed network.

Another difference to the TCA-EDAM is the introduction of a slack load as a substitute for the equivalent impedance of the TCA-EDAM. Hence, the slack load is parameterized to achieve the same steady-state power flow at the boundary bus of the EDAM as at the boundary bus of the detailed network model.

1.3. Contribution and Paper Organization

The STCA is introduced and validated in ref. [7] on an ADN with open ring network topology and six GFMC in different branches of the network. The corresponding EDAM comprise six equivalent GFMC connected in parallel. However, ref. [7] does not analyze the aggregation of multiple GFMC to one equivalent GFMC. Also, the STCA is not applied on a closed ring network topology. Hence, both open research questions are addressed in this work.

To this end, three scenarios differing in network topology and number of GFMC are evaluated. In the first scenario, the STCA is applied on a closed ring network topology with ten GFMC in the detailed network. The second scenario focuses on the aggregation of GFMC. Here, an open ring topology is utilized with eight GFMC in different branches of the network. Two STCA-EDAM are derived from this network: one EDAM with eight equivalent GFMC and one with four equivalent GFMC by clustering the GFMC according to their voltage sensitivities. Each GFMC of the detailed network is in a separate branch of the network. Hence, the aggregation of GFMC necessarily leads to a simplification of the detailed network's topology in the resulting EDAM. The open ring topology of the third scenario

comprises 15 GFMC, all connected to the same network branch. Similar to the second scenario, two STCA-EDAM are evaluated: one EDAM with 15 and one with four equivalent GFMC. Opposed to the second scenario, the detailed network's topology can be considered in the creation of the STCA-EDAM with four equivalent GFMC. All EDAM of the three scenarios are evaluated with respect to model complexity and model validity.

The main contributions of this work are the following: 1) In contrast to other EDAM algorithms that are discussed above, the proposed clustering-based algorithm is not computationally heavy and considers GFMC explicitly. 2) In previous work, STCA-EDAM did not aggregate GFMC. This work evaluates voltage sensitivity clusters for the STCA-EDAM that contain more than one GFMC. 3) Requirements are established to allow for GFMC aggregation in a STCA-EDAM. 4) The STCA is evaluated for closed ring network topologies. 5) The STCA is evaluated for networks with different numbers of GFMC. 6) A method is introduced to allow the comparison of different scenarios in terms of model accuracy and model complexity.

This article introduces the different scenarios, the validation procedure, and the detailed network models of each scenario in Section 2. EDAM of the detailed network models of each scenario are derived and exposed to three different events in Section 3. Also, the dynamic behavior of each EDAM is compared with its corresponding detailed network model by applying a numerical validation. The results of the scenarios are compared and discussed in Section 4. A summary and an outlook conclude this article in Section 5.

2. Methodology

2.1. Simulation Scenario Overview

Three scenarios are investigated in order to analyze and validate the STCA. An overview of the scenarios is shown in **Table 1**. The scenarios differ with respect to ADN topology, number of GFMC in the detailed network, and number of equivalent GFMC in the EDAM. Both TCA and STCA are applied to derive EDAM for a comparison of the STCA with a state-of-the-art approach, i.e., the TCA

Two ADN network topologies are utilized and adapted depending on the scenarios: an open ring (DINGO) and a closed ring (SimBench) topology (Section 2.4). This work focuses on equivalent ADN dominated by CBG, including GFMC. Hence, the CBG share of the models is almost 100% of the ADN's total active power demand. 60% of the CBG's active power generation is covered by GFMC, while the remaining 40% is generated by GFLC. The location within the network and the total number of GFMC vary between the scenarios.

Table 1. Scenario overview.

Scenario name	Network topology	Number of GFMC	Aggregation method	Number of equivalent GFMC (STCA)
SimBench10	SimBench	10	TCA and STCA	10
DINGO8	DINGO	8	TCA and STCA	8 and 4
DINGO15	DINGO	15	TCA and STCA	15 and 4

For this work, GFLC are represented by PV systems and are implemented with two different dynamic models according to Ref. [26]. The generic model for distributed and small as well as for large-scale PV plants differs in their threshold values for disconnection and postfault power generation. GFMC are represented as PV systems with battery storage systems and are modeled as described in Section 2.3. All loads are modeled as constant impedances. Overall, this results in a CBG-dominated network model with a significant influence of GFMC.

The models of each scenario are exposed to three events: a phase angle jump from 0° to 10°, a frequency jump from 50 to 50.25 Hz, and a three-phase short circuit at the PCC of the voltage source as marked in Figure 3. The first two events are induced by the voltage source. All events occur at 0 s, and the short circuit is cleared after 130 ms. The active and reactive power flows at the boundary bus of each EDAM are compared with the power flows at the boundary bus of the corresponding detailed ADN. The software used for the RMS simulations is DigSILENT PowerFactory; the integration time step is chosen to 1 ms.

2.2. Validation Procedure

The evaluation of both TCA- and STCA-based EDAM is realized by a numerical validation procedure that is explained in detail in ref. [7] and is based on the method introduced in ref. [27]. For the three events, both active and reactive power flows at the boundary bus of the EDAM are compared with the active and reactive power flows at the boundary bus of the corresponding detailed network.

For this comparison, three time periods are distinguished: pre-fault (A), fault (B), and post-fault (C). As a fault is defined as a period in which the boundary bus voltage is below 0.9 pu, only the short-circuit event is considered as a fault. The fault period ends with the voltage rising above 0.9 pu. Hence, the responses to a phase angle jump and a frequency jump each are divided in a pre-event (A) and post-event (C) period. The validation is based on the time interval from -1 to 5 s relative to the occurrence of the event.

For each period, the deviation between the dynamic behavior of the EDAM and the detailed network is evaluated based on the active and reactive power flows at the boundary bus normalized by the ADN's total demand, i.e., 40 MW and 10.1 Mvar for the DINGO8 and DINGO15 scenarios, and 31.3 MW and 12.3 Mvar for the SimBench10 scenario (Table 3 and 4). A distinction is made between three different error metrics: mean absolute error δ_{MAE} , mean error δ_{ME} , and maximum error δ_{MXE} . For the exact definition of these metrics, the reader is referred to ref. [7]. The maximum allowed deviations of these three error metrics per time period are listed in **Table 2**.

2.3. Grid Forming Control Model

In this work, the GFMC are modeled with a droop-based approach according to ref. [28]. The GFMC model components are shown on the left-hand side of **Figure 1**. An ideal DC voltage source is connected to a two-level pulse-width modulation (PWM) converter. The PWM converter is then connected to the

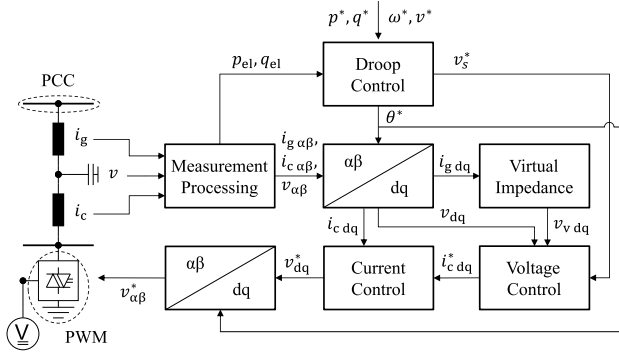


Figure 1. GFMC control according to ref. [28].

Table 2. Threshold values for maximum allowed deviations.^[7,27]

	δ_{MAE}	δ_{ME}	δ_{MXE}
A Prefault	0.12	± 0.10	0.15
B Fault	0.17	± 0.15	0.17
C Postfault	0.17	± 0.15	0.17

grid, i.e., the PCC, via an LCL component filtering harmonics.^[29,30] The filter parameterization depends on the nominal power values of the GFMC according to ref. [30]. The ideal DC voltage source allows for both increasing and decreasing active and reactive power injection. Hence, the GFMC model implemented in this work can be considered as a PV system connected to a battery energy storage system. The storage capacity is assumed to be unlimited for the scenarios considered in this work.

The converter and grid current i_c and i_g , respectively, as well as the voltage v at the capacitor are measured and utilized as inputs for the droop control and Park transformation. Based on set points for the voltage magnitude v^* , angular frequency ω^* , active power p^* , and reactive power q^* , the droop control outputs are set points for voltage angle θ^* and voltage magnitude v_s^* . Here, the superscript $*$ denotes a set point. The grid current in the dq-frame $i_{g,dq}$ is utilized to calculate the voltage $v_{v,dq}$ dependent on the virtual impedance $Z_v = R_v + j\omega L_v$ as

$$v_{v,d} = R_v \cdot i_{g,d} - \omega L_v \cdot i_{g,q} \quad (1)$$

$$v_{v,q} = R_v \cdot i_{g,q} + \omega L_v \cdot i_{g,d} \quad (2)$$

This calculated voltage $v_{v,dq}$, the measured voltage v_{dq} , the measured converter current $i_{c,dq}$, and the droop output voltage magnitude set point v_s^* are inputs to the cascaded voltage and current control. This inner control loop, as shown in Figure 1, is realized with two PI controllers as explained in Ref. [28]. The output is transformed to the $\alpha\beta$ -frame and the resulting voltage $v_{\alpha\beta}^*$ is utilized by the PWM converter.

An important feature of GFMC is the limitation of the output current to protect the converter's power electronics.^[31] The GFMC model implemented in this work utilizes the vector amplitude limitation concept to limit the output current $i_{c,dq}^*$ of the voltage control.^[28] The limited current $i_{c,dq,lim}^*$ reduces both dq components of $i_{c,dq}^*$ simultaneously and is defined as

$$i_{c,dq,lim}^* = \begin{cases} \frac{i_{c,dq}^*}{\sqrt{i_{c,d}^{*2} + i_{c,q}^{*2}}} i_{max}, & \text{if } \sqrt{i_{c,d}^{*2} + i_{c,q}^{*2}} > i_{max} \\ i_{c,dq}^*, & \text{otherwise} \end{cases} \quad (3)$$

2.4. Detailed Network Model

An open ring, i.e., radial, and a closed ring MV ADN test model topology are utilized. In Germany, 84.3% of the MV networks are operated as open ring topologies.^[8] Therefore, greater focus is given to the radial topology in this evaluation. Both ADN topologies are connected to the boundary bus of a transmission system, which is not aggregated, via an extra high voltage (EHV)/medium voltage (MV) transformer. The events as introduced in Section 2.1 are induced by the transmission system. Dependent on the scenario, GFMC are connected to different locations within the network.

Figure 2a shows the transmission system model to which the ADN are connected. It comprises a 230 kV voltage source with a 50 km transmission line. The CIGRE benchmark subtransmission network line parameters in the European configuration^[32] are utilized to parameterize this transmission line.

The open ring ADN topology is based on a 10 kV distribution network of the open-source tool Distribution Network Generator

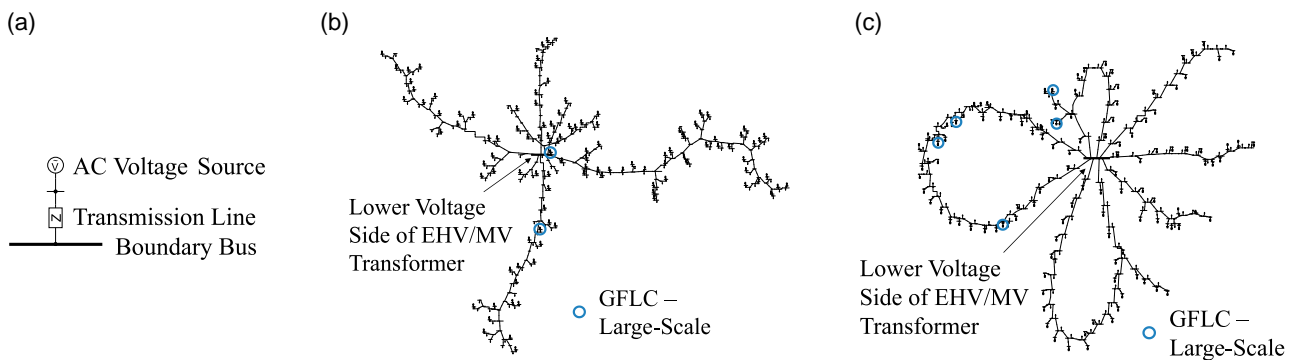


Figure 2. Schematic of a) the transmission system comprising a 230 kV AC voltage source, a transmission line and the boundary bus; b) the 10 kV ADN topology derived from the tool DINGO^[33]; and c) the 20 kV ADN topology derived from the project SimBench.^[37]

(DINGO) that creates synthetic MV networks based on publicly available data of German power system networks.^[33] In this work, one of the MV topologies with a voltage level of 10 kV is selected arbitrarily. The topology of the selected grid represents an urban network and is shown in Figure 2b.

The tool DINGO differentiates between three load areas, whose data are obtained from ref. [34]. Data for conventional and renewable generation are obtained from refs. [35,36]. For this work, the spatial distribution of generators of the resulting synthetic MV network is kept. However, the generation technology is adapted to PV systems with different control strategies to obtain a CBG-dominated urban area. Also, the aggregated load connected at the lower voltage side of the EHV/MV transformer was reduced compared to the MV network obtained from the DINGO tool by 50% to guarantee a more even distribution of the load among the network and avoid a distorting sink at the transformer. The resulting data for the generation and demand are given Table 3.

The closed ring ADN topology is based on a 20 kV distribution network obtained from the project SimBench.^[37] MV networks are compiled synthetically and are categorized into rural, semiurban, urban, and commercial classes. The semiurban MV network is selected arbitrarily for this work. Usually, SimBench networks have an open ring topology. However, three network rings are closed to consider such topology in the STCA evaluation. The resulting network covers a small geographical area with a total line length of 4.7 km and is shown in Figure 2c. Same as for the open ring topology derived from the tool DINGO, the location of generators of the SimBench network is left unchanged. However, generation technology is changed to PV systems with different control strategies. The resulting data for the generation and demand are given in Table 4.

Table 3. Generation and demand data for adapted DINGO MV network.

Component	Number of units	Actual active power [MW]	Actual reactive power [Mvar]
Aggregated load (representing LV area)	1	27.0	6.8
Load > 100 kW	31	10.7	2.7
Load < 100 kW	90	2.3	0.6
Sum	122	40.0	10.1
GFLC—Large-scale	2	9.6	2.0
GFLC—Small	94	6.6	1.3
Sum	96	16.2	3.3

Table 4. Generation and demand data for adapted SimBench MV network.

Component	Number of units	Actual active power [MW]	Actual reactive power [Mvar]
250 kW < Load < 441 kW	43	16.2	6.4
100 kW < Load < 250 kW	64	14.5	5.7
Load < 100 kW	7	0.6	0.2r
Sum	114	31.3	12.3
GFLC—Large-scale	5	5.0	1.0
GFLC—Small	114	7.3	1.5
Sum	119	12.3	2.5

3. Experimental Section

3.1. Scenario: SimBench10

In this section, the closed ring topology with 10 GFMC distributed among the network as shown in Figure 3a is analyzed. All GFMC are attributed with the same nominal values as listed in Table 5.

In this section, two EDAM are compared with each other: an EDAM aggregated by TCA and by STCA. As shown in Table 1, this scenario considers one equivalent GFMC in the STCA-EDAM for each GFMC in the detailed network model. This allows for a consideration of the detailed network's topology. Each closed ring of the detailed network is reproduced by connecting the GFMC of one ring with equivalent impedances. The impedances are then parameterized such that the voltage sensitivities at the PCC of the GFMC in the detailed network match the same at the PCC of the equivalent GFMC in the STCA-EDAM. The resulting EDAM with the same number of equivalent GFMC as the GFMC in the detailed network is shown in Figure 3b.

Two dynamic GFLC control strategies are implemented in the detailed network model. Hence, the STCA-EDAM comprises two equivalent GFLC to address the two control strategies. All loads of the detailed network are constant impedance loads that are represented in the EDAM as one equivalent load. Additionally, a slack load parameterized as described in ref. [7] and Section 1.2.3 is implemented.

In contrast to the STCA-EDAM, the TCA-EDAM comprises one equivalent GFMC representing all GFMC of the detailed network. Also, as stated in Section 1.2.2 and refs. [5,7], instead of a slack load an equivalent impedance minimizes the deviation between the steady-state power flow at the boundary bus of the EDAM and the power flow at the boundary bus of the detailed network model. Figure 3c shows the resulting TCA-EDAM.

The active and reactive power flows at the boundary bus of the detailed network model, the TCA-EDAM, and the STCA-EDAM are shown in Figure 4. For the phase angle jump, the STCA-EDAM reproduces the detailed network's active and reactive power flows very well, whereas the TCA-EDAM results in significant deviations.

Small offsets in the reactive power flow of the STCA-EDAM can be observed for the frequency jump event, while the active power flow matches the one of the detailed network. However, the active and reactive power flows of the TCA-EDAM do not match the ones of the detailed network in the postevent period. Also, the new postevent stationary reactive power set point differs significantly from the stationary reactive power set point of the detailed network.

The reactive power flow at the boundary bus of the STCA-EDAM during and after the short-circuit fault shows a small offset compared to the power flow of the detailed network. The active power flow of the STCA-EDAM captures the power flow of the detailed network very well. The TCA-EDAM shows offsets in the active and reactive power flow during the fault. Also, the postfault behavior differs from the one observed in the detailed network.

The numerical validation confirms the observations (Figure 5). In the pre-event phase, no threshold violations can be observed. During the short-circuit fault, deviations are within limits, except for the reactive power deviation δ_{MXE} of the TCA-EDAM. Validation failure can be observed for the TCA-EDAM in the postevent time period. The frequency jump leads to an active

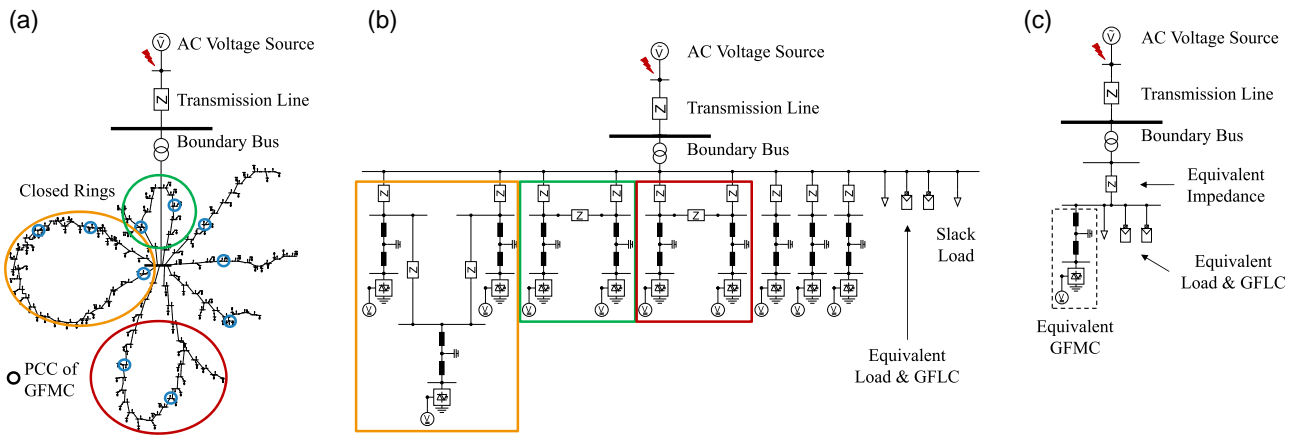


Figure 3. Scenario SimBench10: schematic of a) detailed network with GFMC's PCC, b) of STCA-EDAM, and c) of TCA-EDAM.

Table 5. Scenario Simbench10: GFMC nominal values.

GFMC	Rated apparent power [MVA]	Active power [MW]	Reactive power [Mvar]	Maximum current [pu]
10 GFMC	4	1.9	1	1
Sum	40	19.0	10	–

power threshold violation of the maximum error δ_{MXE} and to a failure of all validation parameters δ_{MAE} , δ_{ME} , and δ_{MXE} for the reactive power deviation. In the postevent period of the phase angle jump and the short circuit, active and reactive power exceeded the allowed maximum deviation δ_{MXE} . Opposed to that, the STCA-EDAM is not exceeding any threshold of the three validation parameters δ_{MAE} , δ_{ME} , and δ_{MXE} for both active and reactive power.

3.2. Scenario: DINGO8

The model utilized in the following scenario builds upon the DINGO grid (Section 2.4) and has one GFMC connected to each of the eight branches of the network as shown in **Figure 6a**.

Due to the increased number of GFMC in this scenario, two STCA-EDAM are compared: 1) STCA 8 GFMC: number of equivalent GFMC, i.e., eight, equals number of GFMC in the detailed network, i.e., eight. 2) STCA 4 GFMC: number of equivalent GFMC, i.e., four, is lower than number of GFMC in the detailed network, i.e., eight.

These two STCA-EDAM are compared with a TCA-EDAM as introduced in Section 1.2.2 and shown exemplarily in **Figure 3c**. As the eight GFMC are located at each of the eight branches of the network, the GFMC of the STCA-EDAM comprising eight GFMC are connected in parallel (**Figure 6b**). Other components besides GFMC are modeled as described for the SimBench10 scenario in Section 3.1.

The GFMC of the detailed network are aggregated to equivalent GFMC in the aggregation level STCA 4 GFMC to avoid a high number of equivalent GFMC. Here, the GFMC in the detailed network are clustered, based on their voltage sensitivities, to the desired number of equivalent GFMC, which is lower than the number of GFMC in the detailed network. However, aggregating multiple GFMC to one equivalent leads to drawbacks, which will be investigated in the following.

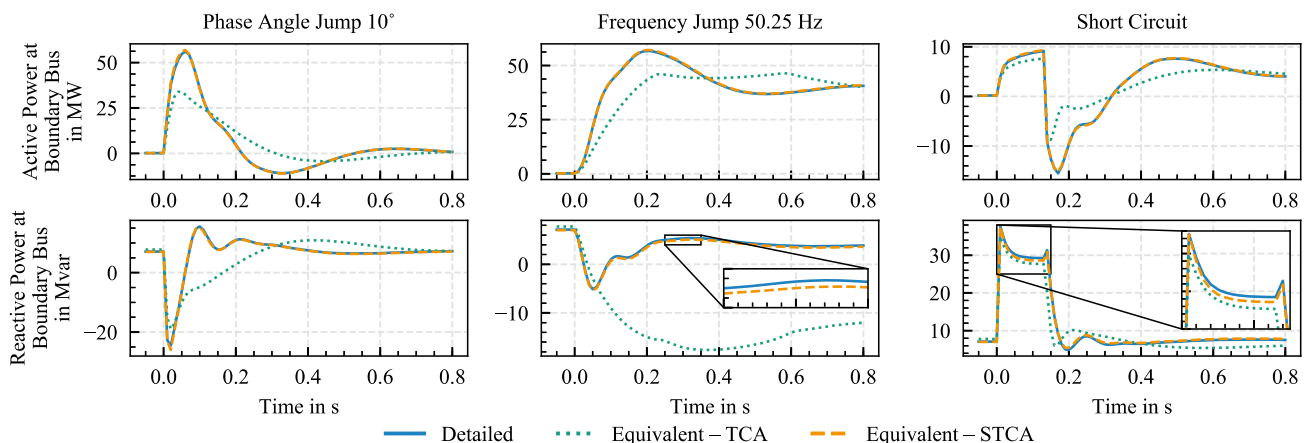


Figure 4. Scenario SimBench10: active and reactive power flow at boundary bus from transmission to distribution system of detailed and equivalent network models; positive reactive power values: overexcited state; negative reactive power values: underexcited state.

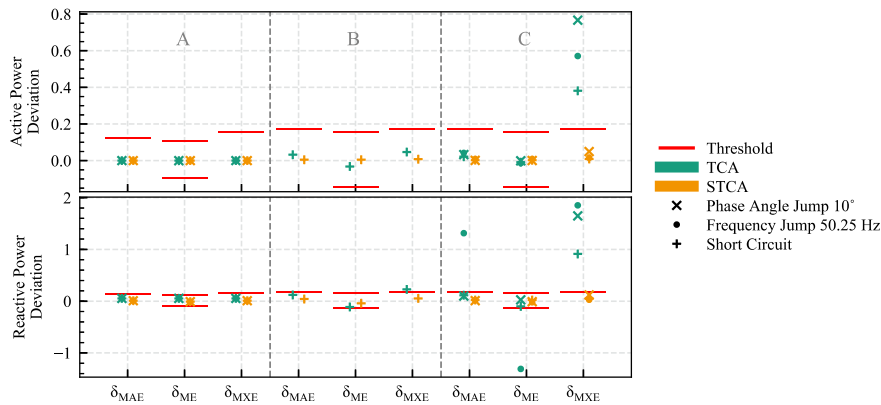


Figure 5. Scenario SimBench10: validation results for EDAM aggregated by TCA and STCA; note that there is no fault period B for the phase angle and frequency jump events.

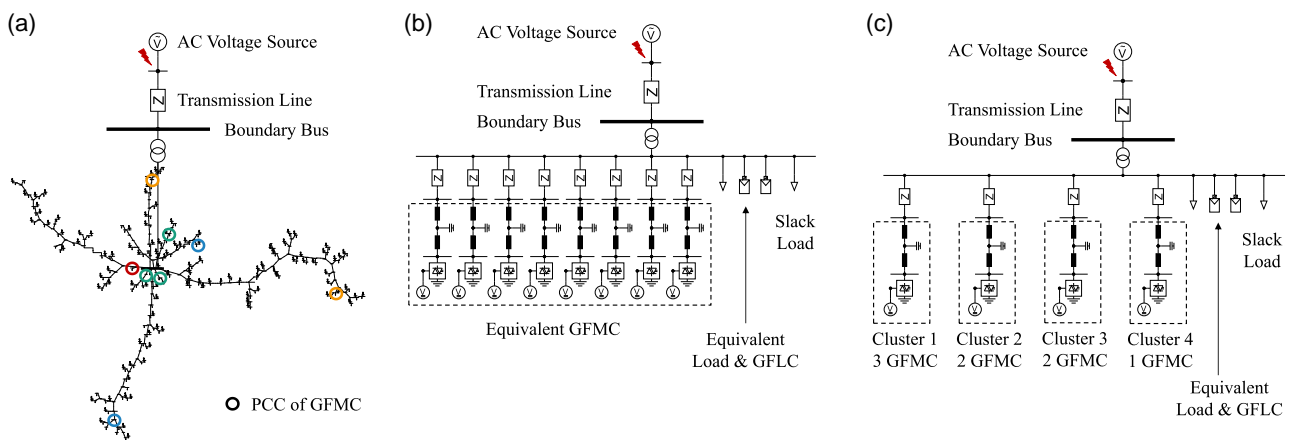


Figure 6. Scenario DINGO8: schematic of a) detailed network with GFMC's PCC colored according to the clusters of the aggregation level STCA 4 GFMC, b) of STCA-EDAM of the aggregation level STCA 8 GFMC, and c) of STCA-EDAM with four GFMC clusters of the aggregation level STCA 4 GFMC.

The *k*-means clustering algorithm^[38,39] finds GFMC clusters with similar voltage sensitivities $\frac{\partial V_i}{\partial P_i}$, $\frac{\partial V_i}{\partial Q_i}$, $\frac{\partial \theta_i}{\partial P_i}$, and $\frac{\partial \theta_i}{\partial Q_i}$. In order to obtain an optimal number of clusters, the total cluster inertia is calculated for different numbers of clusters. Here, inertia is defined as the summed up distances from data points, i.e., voltage sensitivities at the PCC of each GFMC *i*, to their cluster center. Four GFMC clusters are used because only a slight inertia decrease can be observed for a higher number of clusters.

The allocation of GFMC of a cluster in the detailed network can be seen in Figure 6a. While the first cluster (marked green) includes three GFMC, the clusters 2 and 3 contain two GFMC

each (marked orange and blue), and cluster 4 only consists of one GFMC (marked red). It can be seen that the distribution of the GFMC corresponding to the same cluster is not necessarily a neighboring GFMC. The GFMC of cluster 2 (marked orange) are in different network branches. However, they both are located at the branch end, which in this case leads to similar voltage sensitivities.

The resulting EDAM of the aggregation level STCA 4 GFMC is shown in Figure 6c. There are four equivalent GFMC corresponding to the four clusters. The other components are modeled identically to the STCA-EDAM. **Table 6** shows the

Table 6. Scenario DINGO8: equivalent GFMC nominal values.

Aggregation level	GFMC	Rated apparent power [MVA]	Active power [MW]	Reactive power [Mvar]	Maximum current [pu]
STCA 8 GFMC	8 GFMC	5	3	0.75	1
	Sum	40	24	6.00	
STCA 4 GFMC	Cluster 1 (3 GFMC)	15	9	2.25	1
	Cluster 2 and 3 (2 GFMC each)	10	6	1.50	1
	Cluster 4 (1 GFMC)	5	3	0.75	1
	Sum	40	24	6.00	

nominal GFMC values for the STCA-EDAM of both aggregation levels STCA 8 GFMC and STCA 4 GFMC. As multiple GFMC are aggregated to one GFMC, the nominal values of the equivalent GFMC in the STCA-EDAM of the aggregation level STCA 4 GFMC are the summation of the nominal values of the GFMC to be aggregated in the detailed network.

The active and reactive power flows at the boundary bus from the transmission to the detailed ADN model and all three EDAM are shown in **Figure 7**. It can be observed that, for the phase angle jump, the EDAM of the aggregation level STCA 8 GFMC captures both active and reactive power flow of the detailed network very well. The power flows of the TCA-EDAM as well as the STCA-EDAM of the aggregation level 4 GFMC show significant deviations.

Also, the EDAM of the aggregation level STCA 8 GFMC captures the active power flow of the detailed network after the frequency jump very well. The reactive power flow is very close to the detailed network's reactive power flow, despite a small offset. However, the active power flow of the EDAM of the aggregation level STCA 4 GFMC is quite different. The reactive power flow deviates significantly from the one of the detailed networks. While the postevent steady-state reactive power flow of the detailed network is around -3 Mvar, the steady-state value of

the EDAM levels at around -23 Mvar. The TCA-EDAM shows unstable behavior and does not reach stationary active and reactive values after the frequency jump.

The short circuit, being the most severe fault under consideration, causes the biggest deviations between the power flows of the detailed network and the EDAM of the aggregation level STCA 8 GFMC. The active and reactive power flows are similar to those of the detailed network, albeit with a small offset. Besides this offset, the shape is very similar to the shape of the detailed network's active and reactive power flows. The EDAM of the aggregation level STCA 4 GFMC captures the active power flow during the short circuit. However, the EDAM fails to reproduce the detailed network's active power flow in the postfault period. The reactive power flows of the detailed network cannot be captured during and after the fault. Only the postfault steady-state active and reactive power values of the EDAM of the aggregation level STCA 4 GFMC are close to the values of the detailed network. The dynamic active and reactive power flows at the boundary bus of the TCA-EDAM deviates significantly from the same of the detailed ADN model.

These observations are in line with the results of the validation. **Figure 8** shows the validation error metrics δ_{MAE} , δ_{ME} , and δ_{MXE} of the EDAM for all three events. In the pre-event

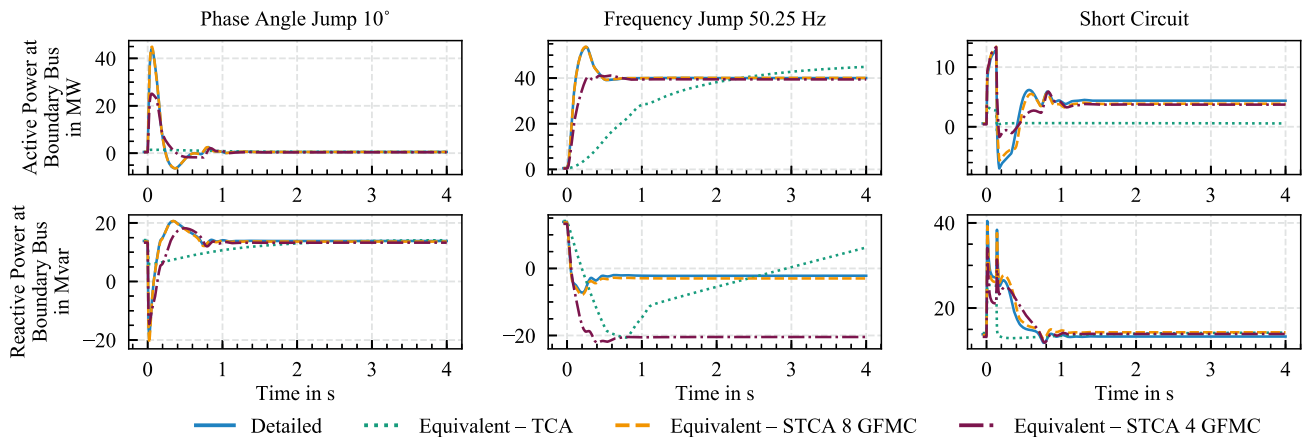


Figure 7. Scenario DINGO8: active and reactive power flow at boundary bus from transmission to distribution system of detailed and equivalent network models; positive reactive power values: overexcited state; negative reactive power values: underexcited state.

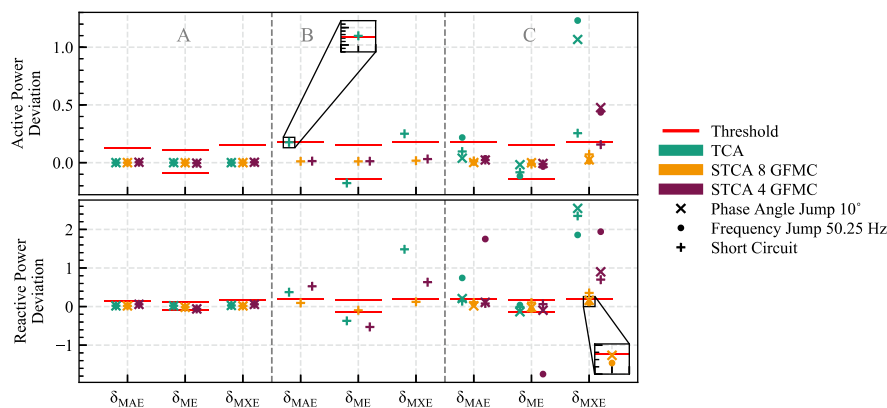


Figure 8. Scenario DINGO8: validation results for TCA-EDAM and STCA-EDAM of both aggregation levels STCA 8 GFMC and STCA 4 GFMC; note that there is no fault period B for the phase angle and frequency jump events.

period A, all error metrics of the three EDAM are close to zero and within the validation limits. This is due to the parameterization of the slack load which yields accurate steady-state pre-event power flows.

During the short-circuit fault (period B), the active power deviation is close to zero for both STCA-EDAM and does not exceed the validation threshold. Opposed to that, the TCA-EDAM is not within the validation limits for all three error metrics. The reactive power deviation of the STCA-EDAM of the aggregation level 8 GFMC is close to the validation limit without exceeding it. The TCA-EDAM and the STCA-EDAM of the aggregation level 4 GFMC fall short of the reactive power validation during the short circuit as all error metrics exceed their corresponding threshold.

Active power deviations in the postevent period C of the EDAM of the aggregation level STCA 8 GFMC are within the validation limits for all three events and error metrics. The EDAM of the aggregation level STCA 4 GFMC also passes the validation for the error metrics δ_{MAE} and δ_{ME} in all three events. Opposed to that, the active power deviation exceeds the threshold for the maximum error δ_{MXE} in the postevent period of the phase angle and frequency jump. The TCA-EDAM is within the validation limits for δ_{MAE} in the postevent period of the phase angle jump and the short circuit as well as for δ_{ME} in all three events.

Reactive power deviations in the postfault period of the short-circuit cause δ_{MXE} of the EDAM of the aggregation level STCA 8 GFMC to exceed the validation limit, while the other events do not lead to any validation threshold violation. Opposed to that, the frequency jump leads to validation failures of the EDAM of the aggregation level STCA 4 GFMC in the postevent period for all three error metrics, while δ_{MXE} exceeds the threshold value in the postevent period for all three events. The reactive power deviations of the TCA-EDAM are within the validation limits for δ_{MAE} in the postevent period of the short circuit and for δ_{ME} in all three events.

It can be seen that especially the reactive power flow after the frequency jump event of the STCA-EDAM with four equivalent GFMC differs significantly from the reactive power flow of the detailed network. This indicates that the aggregation of non-neighboring GFMC yields STCA-EDAM that do not reproduce

the dynamic behavior of the corresponding detailed network well.

3.3. Scenario: DINGO15

The results of scenario DINGO8 show that an aggregation of multiple GFMC to a fewer number of equivalent GFMC results in performance drawbacks of the STCA. The consideration of GFMC in a STCA-EDAM depends on the network topology of the detailed network.^[7] However, by aggregating multiple non-neighboring GFMC, the detailed network's topology cannot be taken into account in the EDAM.

Nevertheless, in the case of networks with a high number of GFMC in one branch or one closed ring, the aggregation of neighboring GFMC within this branch or closed ring can result in a significant complexity reduction and the detailed network's topology can still be considered in the EDAM. This case is investigated in the following scenario.

Here, a detailed network with 15 GFMC in one branch of the DINGO network topology (Section 2.4) as shown in **Figure 9a** is considered. Similar to the scenario DINGO8, a STCA-EDAM with 15 equivalent GFMC is compared to a STCA-EDAM with four GFMC: 1) STCA 15 GFMC: number of equivalent GFMC, i.e., 15, equals number of GFMC in the detailed network, i.e., 15. 2) STCA 4 GFMC: number of equivalent GFMC, i.e., four, is lower than number of GFMC in the detailed network, i.e., 15.

The STCA-EDAM of both aggregation levels are compared with a TCA-EDAM for benchmarking purposes. The resulting TCA-EDAM is similar to the STCA-EDAM but with all GFMC aggregated as one equivalent GFMC.

For the aggregation level STCA 15 GFMC, the GFMC location in the detailed network needs to be considered as described in ref. [7], resulting in the connection of the equivalent GFMC with equivalent impedances as shown in Figure 9b. The other components, i.e., loads and GFLC, are aggregated as described in Section 3.1.

For the aggregation level STCA 4 GFMC, the GFMC are clustered according to their voltage sensitivities $\frac{\partial V_i}{\partial P_i}$, $\frac{\partial V_i}{\partial Q_i}$, $\frac{\partial \theta_i}{\partial P_i}$, and $\frac{\partial \theta_i}{\partial Q_i}$ as

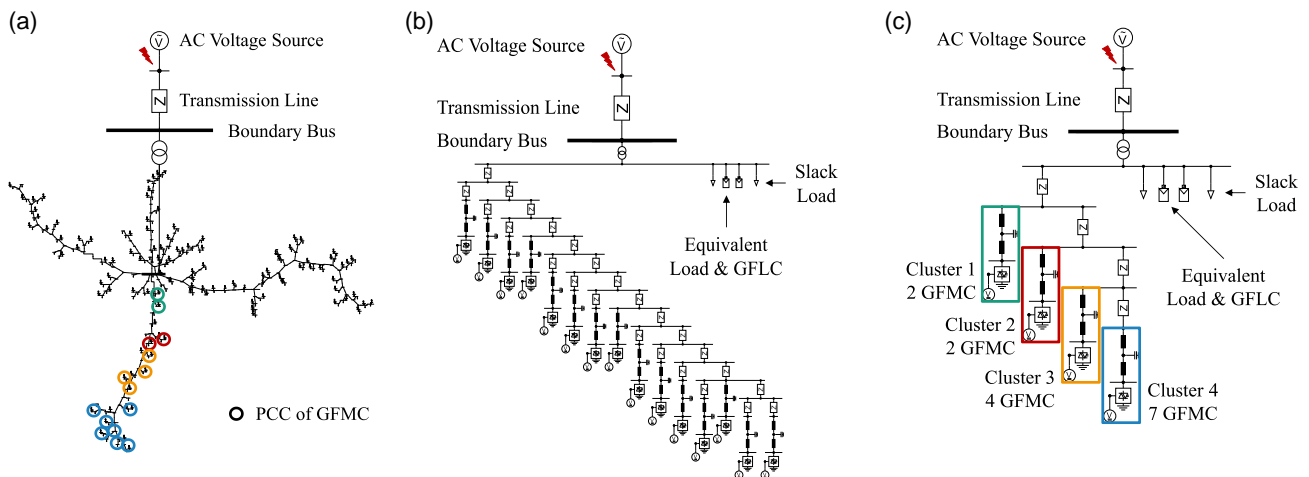


Figure 9. Scenario DINGO15: schematic of a) detailed network with GFMC's PCC colored according to the clusters of the aggregation level STCA 4 GFMC, b) of STCA-EDAM of the aggregation level STCA 15 GFMC, and c) of STCA-EDAM with four GFMC clusters of the aggregation level STCA 4 GFMC.

described in Section 3.2. To identify the optimal number of clusters, the total cluster inertia is calculated for different number of clusters. Here, only marginal inertia improvements can be observed for more than four clusters. Hence, four GFMC clusters are defined for this aggregation level. The PCC of GFMC of the same cluster are colored accordingly in Figure 9a.

The resulting EDAM of the aggregation level STCA 4 GFMC is shown in Figure 9c. The network topology of the detailed model could be kept because only neighboring GFMC of one branch are in one cluster. The number of aggregated GFMC in the detailed network and the nominal values of the equivalent GFMC of each aggregation level are listed in Table 7.

Figure 10 shows the active and reactive power flows at the boundary bus of the detailed ADN model, the TCA-EDAM, and the STCA-EDAM of both aggregation levels STCA 15 GFMC and STCA 4 GFMC. It can be observed that the active power flow after the phase angle jump of the EDAM of the aggregation level STCA 15 GFMC is very similar compared to the detailed network, whereas the EDAM with the aggregated GFMC of the aggregation level STCA 4 GFMC differs slightly. Especially the active power peak following the phase angle jump cannot be captured fully by the EDAM of the aggregation level STCA 4 GFMC.

Similarly, the reactive power flow after the phase angle jump of the EDAM of the aggregation level STCA 15 GFMC and of the aggregation level STCA 4 GFMC captures the dynamic behavior of the detailed network very well. Small deviations, however, can

be observed for the latter. Opposed to that, the TCA-EDAM does not capture the detailed network's dynamic behavior for both active and reactive power adequately.

The EDAM of the aggregation level STCA 15 GFMC exposed to the frequency jump leads to an active and reactive power flow at the boundary bus that is very similar to the corresponding power flow of the detailed network. However, the EDAM of the aggregation level STCA 4 GFMC slightly deviates from the detailed network's dynamic behavior. Nevertheless, the deviations are less distinct compared to the deviations of the TCA-EDAM. Both active and reactive power flows of the detailed network are not reproduced well.

As observed with the other events, the dynamic behavior of the detailed network during and after the short circuit is captured by STCA-EDAM of both aggregation levels, whereas the EDAM of the aggregation level STCA 15 GFMC reproduces the detailed network's behavior more distinctly. Opposed to that, the dynamic behavior of the TCA-EDAM deviates significantly from the behavior of the detailed network for both active and reactive power. The numerical validation is applied and described in the following paragraphs to quantify these deviations.

Figure 11 shows the validation results for active and reactive power deviations of the TCA-EDAM and STCA-EDAM of both aggregation levels. It can be seen that both STCA-EDAM do not exceed any validation threshold of active and reactive power deviation for all three events.

Table 7. Scenario DINGO15: equivalent GFMC nominal values.

Aggregation level	GFMC	Rated apparent power [MVA]	Active power [MW]	Reactive power [Mvar]	Maximum current [pu]
STCA 15 GFMC	20 GFMC	2.5	1.6	0.4	1
	Sum	37.5	24.0	6.0	
STCA 4 GFMC	Cluster 1 and 2 (2 GFMC each)	5.0	3.2	0.8	1
	Cluster 3 (4 GFMC)	10.0	6.4	1.6	1
	Cluster 4 (7 GFMC)	17.5	11.2	2.8	1
	Sum	37.5	24.0	6.0	

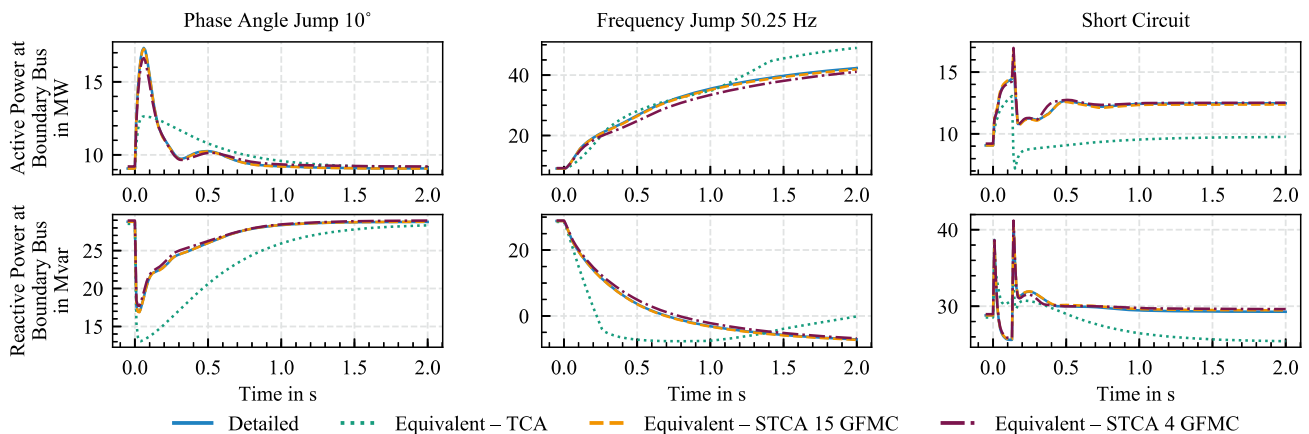


Figure 10. Scenario DINGO15: active and reactive power flow at boundary bus from transmission to distribution system of detailed and equivalent network models; positive reactive power values: overexcited state; negative reactive power values: underexcited state.

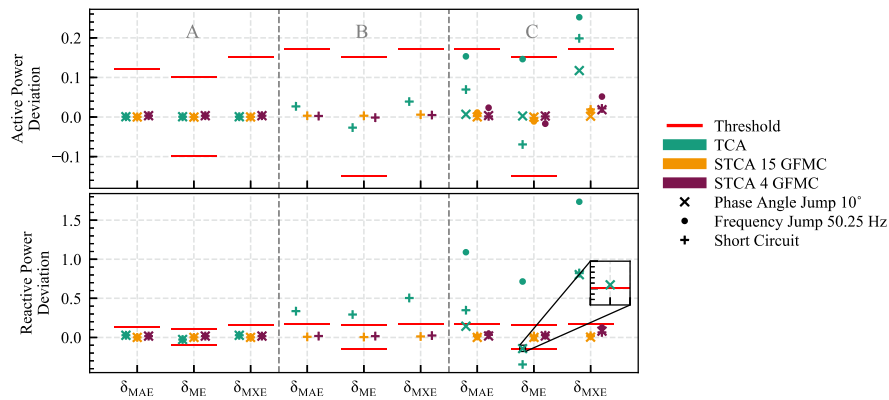


Figure 11. Scenario DINGO15: validation results for TCA-EDAM and STCA-EDAM of both aggregation levels STCA 15 GFMC and STCA 4 GFMC; note that there is no fault period B for the phase angle and frequency jump events.

Opposed to that, the TCA-EDAM exceeds validation limits for the active power deviation δ_{MXE} in the postevent period C of the frequency jump and the short circuit. The validation of all error metrics of reactive power deviation is failed by the TCA-EDAM during and after the short circuit. Also, the threshold values of all reactive power deviation error metrics are exceeded in the postevent period C of the frequency jump. Additionally, the reactive power deviation δ_{MXE} exceeds the allowed validation limit in the postevent period of the phase angle jump.

4. Discussion

In this section, the model complexity of each of the different EDAM created for the scenarios in Section 3 is evaluated and put into relation to its respective accuracy. For comparison purposes, the error metrics of Section 2.2 are condensed to accuracy indicators. Here, the complexity of a model is assessed by the computation time needed to simulate it from -5 to 5 s and by its number of nodes.

In **Table 8**, the reduction of the EDAM complexity in terms of simulation time and number of nodes in relation to the

Table 8. Model complexity of EDAM exposed to a short-circuit fault.

Scenario	Distribution network model		Simulation time
	Aggregation method	Number of nodes	Relative to the detailed model
SimBench10	None (detailed model)	114	100.0%
	TCA	2	1.4%
	STCA	11	5.4%
DINGO8	None (detailed model)	195	100.0%
	TCA	2	1.6%
	STCA 4 GFMC	5	4.7%
	STCA 8 GFMC	9	7.8%
DINGO15	None (detailed model)	195	100.0%
	TCA	2	1.4%
	STCA 4 GFMC	5	4.1%
	STCA 15 GFMC	26	5.5%

corresponding detailed network model is investigated. The short circuit as the most severe fault was utilized to evaluate the simulation time. It is important to mention that nodes considered to be part of a component are not taken into account for this evaluation, e.g., due to the LCL filter, the PWM component, and the DC voltage source, the GFMC component comprises multiple nodes which are not considered.

The reduction in the number of nodes and simulation time is significant for all EDAM of all scenarios. In the TCA-EDAM, all GFMC of the detailed network are aggregated to one equivalent GFMC. This leads to few components in the EDAM and, therefore, to a speedy simulation needing only down to 1.4% of the detailed network's simulation time.

The STCA-EDAM with less equivalent GFMC than the GFMC in the detailed network reduces the complexity significantly. In the scenarios DINGO8 and DINGO15, the GFMC were aggregated to four equivalent GFMC clusters resulting in five nodes in the EDAM. The low number of equivalent components also reduces the simulation time up to 4.1% of the detailed network's simulation time.

When all GFMC of the detailed network are considered in the STCA-EDAM, the number of nodes is higher than for the other EDAM. Considering the network's topology necessitates implementing intersection nodes in the EDAM. To this end, the EDAM of scenario DINGO15 comprising 15 GFMC consists of 26 nodes. However, the STCA-EDAM's complexity reduction remains significant compared to the detailed network's number of nodes (195) and simulation time.

In the following paragraphs, the model complexity is put into relation to the model accuracy. In order to enable a comparison between number of nodes, simulation time, and the validation results, the error metrics δ_{MAE} , δ_{ME} , and δ_{MXE} of each scenario are condensed to qualitative accuracy indicators ν_{P_MAE} , ν_{P_ME} , ν_{P_MXE} , ν_{Q_MAE} , ν_{Q_ME} , and ν_{Q_MXE} .

The definition of these accuracy indicators is introduced in the following. As explained in Section 2.2, phase angle and frequency jump simulation results are divided into a pre-event and postevent phase, whereas the results for the short-circuit fault are categorized in a pre-fault, fault, and postfault period. For each period and for each event, there is one corresponding active and reactive power error metric δ_{MAE} , δ_{ME} , and δ_{MXE} . Hence, each active or

reactive power deviation error metric is calculated seven times per event ($N = 7$). These seven metrics can be put into a vector. As an example, the vector δ_{P_MAE} is represented by the individual active power error metric δ_{MAE} per event and period, that is

$$\delta_{P_MAE} = \begin{pmatrix} |\delta_{P_MAE_ph_A}| \\ |\delta_{P_MAE_ph_C}| \\ |\delta_{P_MAE_fr_A}| \\ |\delta_{P_MAE_fr_C}| \\ |\delta_{P_MAE_sc_A}| \\ |\delta_{P_MAE_sc_B}| \\ |\delta_{P_MAE_sc_C}| \end{pmatrix}, \quad (4)$$

where 1) $\delta_{P_MAE_ph_A}$: active power (P) error metric δ_{MAE} in the pre-event time period (A) of the phase angle jump (ph). 2) $\delta_{P_MAE_ph_C}$: active power (P) error metric δ_{MAE} in the postevent time period (C) of the phase angle jump (ph). 3) $\delta_{P_MAE_fr_A}$: active power (P) error metric δ_{MAE} in the pre-event time period (A) of the frequency jump (fr). 4) $\delta_{P_MAE_fr_C}$: active power (P) error metric δ_{MAE} in the postevent time period (C) of the frequency jump (fr). 5) $\delta_{P_MAE_sc_A}$: active power (P) error metric δ_{MAE} in the pre-fault time period (A) of the short circuit (sc). 6) $\delta_{P_MAE_sc_B}$: active power (P) error metric δ_{MAE} in the fault time period (B) of the short circuit (sc). 7) $\delta_{P_MAE_sc_C}$: active power (P) error metric δ_{MAE} in the postfault time period (C) of the short circuit (sc). As δ_{ME} is the only metric that can be negative, taking the absolute values in (4) is in fact only relevant for δ_{P_ME} and δ_{Q_ME} . The individual error metrics of each vector are summed up and the average deviation is calculated. This average is normalized such that the value 100% means that the EDAM matches the detailed network perfectly for the respective error metric. The resulting qualitative accuracy indicator ν_{P_MAE} then is defined as

$$\nu_{P_MAE} = \max \left\{ 0\%, \left(1 - \frac{1}{N} \sum_{i=1}^N \delta_{P_MAE}(i) \right) \cdot 100\% \right\} \quad (5)$$

where $\delta_{P_MAE}(i)$ is the vector of (4) and $N = 7$ is the length of that vector.

The other accuracy indicators ν_{P_ME} , ν_{P_MXE} , ν_{Q_MAE} , ν_{Q_ME} , and ν_{Q_MXE} are calculated accordingly with the vectors $\delta_{P_ME}(i)$, $\delta_{P_MXE}(i)$, $\delta_{Q_MAE}(i)$, $\delta_{Q_ME}(i)$, and $\delta_{Q_MXE}(i)$, respectively. The indices P and Q indicate error metrics corresponding to active and reactive power deviation, respectively.

In **Figure 12**, the two model complexity indicators, i.e., simulation time and number of nodes, are compared to the six accuracy indicators as introduced in Equation (5). The simulation time and the number of nodes are normalized such that 100% corresponds to the simulation time and the number of nodes, respectively, of the detailed network. Each plot is related to one of the three scenarios introduced in Section 2.1. As this evaluation is qualitative, for quantitative results, it is recommended to check the validation results in the respective section in Section 3 and the model complexity listed in Table 8.

Two EDAM were considered in the *SimBench10* scenario: TCA-EDAM and the STCA-EDAM with the same amount of equivalent GFMC compared to the GFMC in the detailed network. The model complexity indicators, i.e., simulation time and the number of nodes, of the STCA-EDAM are slightly higher than the TCA-EDAM complexity. However, this model complexity reduction of the TCA-EDAM results in a notable deviation from the detailed network for the accuracy indicators ν_{P_MXE} , ν_{Q_MAE} , ν_{Q_ME} , and ν_{Q_MXE} . The STCA-EDAM is very close to 100% for all accuracy indicators except ν_{Q_MXE} , where a slight deviation can be observed.

In the scenario DINGO8, one TCA-EDAM and two STCA-EDAM (4 GFMC and 8 GFMC) are compared. Minor differences in model complexity can be observed between the EDAM. Nevertheless, the EDAM accuracy differs significantly. The TCA-EDAM does not reach a stationary reactive power value in the postevent period of the frequency jump, resulting in a seemingly high model accuracy with regard to the indicator ν_{Q_ME} . However, this is due to the partial compensation of negative and positive deviations of the TCA-EDAM as can be seen in

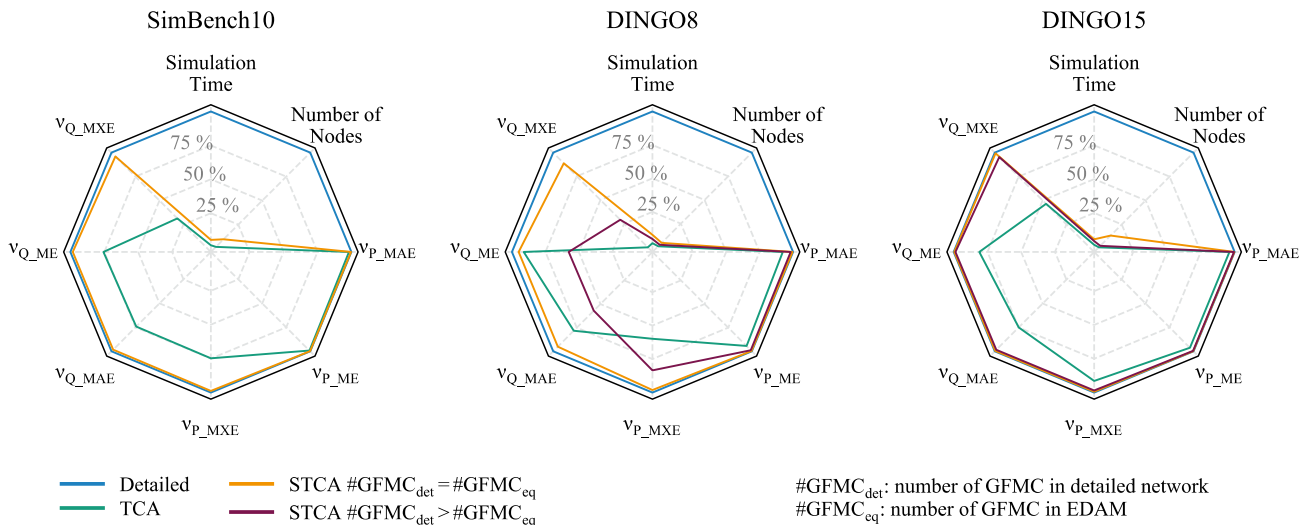


Figure 12. Comparison of model complexity indicators, i.e., simulation time and number of nodes, and accuracy indicators of the scenarios described in Section 3 (SimBench10, DINGO8, DINGO15).

Figure 7. In fact, ν_{Q_MXE} reaches even 0 and shows the poor reproduction of the detailed network's dynamic behavior. Also, the model STCA 4 GFMC has severe accuracy drawbacks, in particular for the parameters ν_{P_MXE} , ν_{Q_MAE} , ν_{Q_ME} , and ν_{Q_MXE} , while the STCA 8 GFMC performs well.

This is different for the STCA 4 GFMC EDAM of scenario DINGO15, in which only neighboring GFMC of one network branch are aggregated and the detailed network's topology is considered. Here, only minor deviations between the two STCA-EDAM can be observed with respect to the accuracy indicators, whereas the model complexity is higher for the EDAM in which no GFMC of the detailed network is aggregated. The TCA-EDAM also fails to reproduce the detailed network's dynamic behavior especially for reactive power, resulting in low accuracy indicators.

By assessing the qualitative deviations of the EDAM from the detailed network for each scenario, it becomes clear that all EDAM reduce the complexity of the detailed model remarkably. The higher the number of GFMC in the detailed network, the higher is the STCA-EDAM's model complexity that considers each GFMC individually. Nevertheless, this higher EDAM complexity has to be put in relation to the reasonably accurate representation of the detailed network's dynamic behavior. Unless multiple GFMC are in one branch of the network allowing the aggregation of neighboring GFMC, the STCA-EDAM with aggregated equivalent GFMC deviates significantly from the detailed network. Also, the TCA-EDAM reduces the model complexity the most, but is not able to capture the dynamic behavior of the detailed network for any of the considered network scenarios.

5. Conclusion and Outlook

Previous work introduces the STCA as a method to derive EDAM of CBG-dominated networks including GFMC.^[7] The STCA clusters GFMC in the detailed network according to the voltage sensitivities $\frac{\partial V_i}{\partial P_i}$, $\frac{\partial V_i}{\partial Q_i}$, $\frac{\partial \theta_i}{\partial P_i}$, and $\frac{\partial \theta_i}{\partial Q_i}$ at the PCC of each GFMC i . In ref. [7], GFMC are considered individually in the EDAM, i.e., each voltage sensitivity cluster comprises exactly one GFMC in order to connect the equivalent GFMC according to the detailed network's topology. Additionally, previous work focuses on an open ring network topology.^[7]

This article addresses open research questions in the STCA evaluation. In the scenario SimBench10, the STCA is evaluated on a closed ring topology. The closed rings of the detailed network are considered in the EDAM and the STCA-EDAM reproduces the dynamic behavior of the detailed network model very well for the considered events. Additionally, the aggregation of multiple GFMC to one equivalent GFMC by clustering according to voltage sensitivities is investigated in the scenario DINGO8. In this scenario, the clustering leads to an aggregation of non-neighboring GFMC in one network branch. Hence, a consideration of the detailed network's topology in the EDAM is not possible, which results in a different dynamic GFMC response to faults. To address this challenge, this work proposes a constraint for the GFMC aggregation to allow a topology consideration in the EDAM. Only neighboring GFMC of one network branch with similar voltage sensitivities should be aggregated to an equivalent

component. Hence, the clustering of GFMC must be performed for each network branch or closed ring individually. The scenario DINGO15 investigates such a GFMC aggregation and shows the validity of the resulting EDAM with aggregated GFMC.

The application of the STCA is evaluated in different scenarios and constraints are established for the aggregation of multiple GFMC to one equivalent component. Hence, the STCA is most suitable for stability analysis of a future power system with a significant amount of CBG including GFMC. The STCA can be applied on network models with different topologies as well as different numbers of GFMC. Varying both parameters is important when conducting comprehensive stability analysis.

This work focuses on a sensitivity clustering of GFMC only. Nevertheless, the representation of voltage-dependent GFLC control in an EDAM may be improved by a GFLC clustering according to voltage sensitivities. Future work should analyze the advantages of such an approach. Further work should also investigate the application of the STCA on an ADN comprising both low and medium voltage networks. The STCA could be applied in a bottom-up way, starting with the aggregation of the low voltage network.

Acknowledgements

The work presented in this paper has been supported by the German Federal Ministry for Education and Research (BMBF) within the scope of the research project "RESIST—Resiliente Stromnetze für die Energiewende" (FKZ 03SF0637).

Open Access funding enabled and organized by Projekt DEAL.

Conflict of Interest

The authors declare no conflict of interest.

Data Availability Statement

The data that support the findings of this study are available from the corresponding author upon reasonable request.

Keywords

active distribution networks, distributed generation, distributed network equivalent, equivalent dynamic models, gray-box approach, grid forming converter

Received: March 29, 2023

Revised: April 26, 2023

Published online: May 26, 2023

- [1] G. Chaspierre, G. Denis, P. Panciatici, T. Van Cutsem, *IEEE Open Access J. Power Energy* **2021**, 8, 497.
- [2] Z. Liu, N. Bornhorst, S. Wende-von Berg, M. Braun, in *IEEE Conf. on Sustainable Energy Supply and Energy Storage Systems (NEIS)*, Hamburg, **2020**.
- [3] S. M. Zali, J. V. Milanovic, *IEEE Trans. Power Syst.* **2013**, 28, 3126.
- [4] Joint Working Group C4/C6.35/C1RED. Modelling of Inverter-Based Generation for Power System Dynamic Studies. Technical Report, CIGRE, **2018**.

- [5] J. C. Bömer. Ph.D. Thesis, Technische Universiteit Delft, **2016**.
- [6] ENTSO-E Technical Group on High Penetration of Power Electronic Interfaced Power Sources. High Penetration of Power Electronic Interfaced Power Sources and the Potential Contribution of Grid Forming Converters. Technical report, ENTSO-E, https://www.entsoe.eu/Documents/Publications/SOC/High_Penetration_of_Power_Electronic_Interfaced_Power_Sources_and_the_Potential_Contribution_of_Grid_Forming_Converters.pdf, (accessed: April 2022).
- [7] J. Ungerland, N. Poshuya, W. Biener, H. Lens, *IEEE Trans. Smart Grid* **2022**.
- [8] J. Büchner, J. Katzfey, O. Flörcken, A. Moser, H. Schuster, S. Dierkes, T. van Leeuwen, L. Verheggen, M. Uslar, M. van Amelsvoort, Moderne Verteilernetze für Deutschland (Verteilernetzstudie). Technical Report, Vol 44, **2014**.
- [9] J. Ungerland, R. Bhadani, W. Biener, H. Lens, in *13th IEEE Int. Symp. on Power Electronics for Distributed Generation Systems (PEDG)*, IEEE, Piscataway, NJ **2022**.
- [10] S. M. Zali, Ph.D. Thesis, University of Manchester, **2012**.
- [11] X. Wu, Ph.D. Thesis, RWTH Aachen University, **2016**.
- [12] J. M. R. Arredondo, *Int. J. Electr. Power Energy Syst.* **1999**, 21, 365.
- [13] F. O. Resende, J. Matevosyan, J. V. Milanovic, in *IEEE Grenoble Conf. PowerTech*, IEEE, Piscataway, NJ **2013**.
- [14] P. Dimo, *Edit. Acad. Republic. Social. România* **1975**.
- [15] E. J. Davison, *IEEE Trans. Autom. Control* **1966**, 11, 93.
- [16] G. Mitrentsis, H. Lens, *IEEE Trans. Smart Grid* **2021**, 12, 2952.
- [17] F. Conte, F. D'Agostino, F. Silvestro, *Electric Power Syst. Res.* **2019**, 168, 92.
- [18] X. Shang, Z. Li, J. Zhang, Q. H. Wu, *Int. J. Electr. Power Energy Syst.* **2019**, 112, 83.
- [19] N. Fulgêncio, C. Moreira, L. Carvalho, J. A. Peças Lopes, *Electr. Power Syst. Res.* **2020**, 178.
- [20] X. Wu, X. Lei, Y. Lan, A. Monti, F. Gao, in *IEEE Int. Conf. on Power System Technology, POWERCON*, IEEE, Piscataway, NJ **2018**, pp. 529–536.
- [21] A. Ishchenko, J. M. Myrzik, W. L. Kling. *IET Gen. Transmis. Distrib.* **2007**, 1, 818.
- [22] X. Feng, Z. Lubosny, J. W. Bialek, in *IEEE Lausanne Power Tech*, IEEE, Piscataway, NJ **2007**, pp. 267–272.
- [23] A. M. Azmy, I. Erlich, P. Sowa. *IET Proc. Gen. Transmis. Distrib.* **2004**, 151, 681.
- [24] G. Lammert, K. Yamashita, L. D. P. Ospina, H. Renner, S. M. Villanueva, P. Pourbeik, F.-E. Ciausiu, M. Braun. *CIGRE Sci. Eng. J.* **2017**, 8, 25.
- [25] M. F. Valois-Rodriguez, J. Ungerland. in *IEEE PES Innovative Smart Grid Technologies Europe (ISGT-Europe)*, IEEE, Piscataway, NJ **2020**, pp. 824–828.
- [26] WECC Renewable Energy Modeling Task Force, WECC PV Power Plant Dynamic Modeling Guide. Technical Report, WECC, <https://www.wecc.org/Reliability/WECC%20Solar%20Plant%20Dynamic%20Modeling%20Guidelines.pdf>, (accessed: April 2022).
- [27] FGW, Technische Richtlinien für Erzeugungseinheiten: Teil 4. Technical Report, FGW e.V. Fördergesellschaft Windenergie und andere Dezentrale Energien, Berlin **2019**.
- [28] P. N. Pham, A. Salman, R. Singer, in *Solar Integration Workshop, Energynautics GmbH, Darmstadt, Germany* **2020**.
- [29] M. Liserre, F. Blaabjerg, S. Hansen. *IEEE Trans. Ind. Appl.* **2005**, 41, 1281.
- [30] A. Reznik, M. G. Simoes, A. Al-Durra, S. M. Mueyen, *IEEE Trans. Ind. Appl.* **2014**, 50, 1225.
- [31] M. G. Taul, X. Wang, P. Davari, F. Blaabjerg. *IEEE J. Emerg. Select. Topics Power Electron.* **2020**, 8, 1062.
- [32] K. Strunz, E. Abbasi, C. Abbey, C. Andrieu, R. C. Campbell, R. Fletcher, Benchmark Systems for Network Integration of Renewable and Distributed Energy Resources. Technical Report April, CIGRE, **2014**.
- [33] J. Amme, G. Pleßmann, J. Bühler, L. Hülk, E. Kötter, P. Schwaegerl. *J. Phys. Conf. Ser.* **2018**, 977.
- [34] L. Hülk, L. Wienholt, I. Cußmann, U. P. Mueller, C. Matke, E. Koetter. *Int. J. Sustain. Energy Plan. Manage.* **2017**, 13, 79.
- [35] Bundesnetzagentur, List of Power Plants. Technical Report, <https://www.bundesnetzagentur.de/EN/Areas/Energy/Companies/SecurityOfSupply/GeneratingCapacity/PowerPlantList/start.html>, (accessed: April 2022).
- [36] Deutsche Gesellschaft für Sonnenenergie e.V. Die EEG-Anlagen der Region Bundesrepublik Deutschland (EnergyMap), **2014**.
- [37] S. Meinecke, D. Sarajlic, S. R. Drauz, A. Klettke, L. P. Lauen, C. Rehtanz, A. Moser, M. Braun, *Energies*, **2020**, 13.
- [38] J. MacQueen. in *5th Berkeley Symp. on Mathematical Statistics and Probability*, (Eds: L. M. Le Cam, J. Neyman), Vol 1, University of California Press, Oakland, CA **1967**, pp. 281–297.
- [39] S. P. Lloyd, *IEEE Trans. Inform. Theory* **1982**, 28, 129.